Published in final edited form as:
*Neuroimage*. 2014 January 1; 84: 534–545. doi:10.1016/j.neuroimage.2013.08.069.

# Visualization of intra-thalamic nuclei with optimized white-matter-nulled MPRAGE at 7T

**Thomas Tourdias**[a,1], **Manojkumar Saranathan**[a], **Ives R. Levesque**[a], **Jason Su**[a], and **Brian K. Rutt**[a]

[a] Richard M. Lucas Center for Imaging Radiology Department Stanford University 1201 Welch Road Stanford, California USA 94305-5488

## Abstract

Novel MR image acquisition strategies have been investigated to elicit contrast within the thalamus, but direct visualization of individual thalamic nuclei remains a challenge because of their small size and the low intrinsic contrast between adjacent nuclei. We present a step-by-step specific optimization of the 3D MPRAGE pulse sequence at 7T to visualize the intra-thalamic nuclei. We first measured T1 values within different sub-regions of the thalamus at 7T in 5 individuals. We used these to perform simulations and sequential experimental measurements (n=17) to tune the parameters of the MPRAGE sequence. The optimal set of parameters was used to collect high-quality data in 6 additional volunteers. Delineation of thalamic nuclei was performed twice by one rater and MR-defined nuclei were compared to the classic Morel histological atlas. T1 values within the thalamus ranged from 1400ms to 1800ms for adjacent nuclei. Using these values for theoretical evaluations combined with *in vivo* measurements, we showed that a short inversion time (TI) close to the white matter null regime (TI=670ms) enhanced the contrast between the thalamus and the surrounding tissues, and best revealed intra-thalamic contrast. At this particular nulling regime, lengthening the time between successive inversion pulses (TS=6000ms) increased the thalamic signal and contrast and lengthening the $\alpha$ pulse train time (N*TR) further increased the thalamic signal. Finally, a low flip angle during the gradient echo acquisition ($\alpha$=4°) was observed to mitigate the blur induced by the evolution of the magnetization along the $\alpha$ pulse train. This optimized set of parameters enabled the 3D delineation of 15 substructures in all 6 individuals; these substructures corresponded well with the known anatomical structures of the thalamus based on the classical Morel atlas. The mean Euclidean distance between the centers of mass of MR- and Morel atlas-defined nuclei was 2.67mm (±1.02mm). The reproducibility of the MR-defined nuclei was excellent with intraclass correlation coefficient measured at 0.997 and a mean Euclidean distance between corresponding centers of mass found at first versus second readings of 0.69mm (±0.38mm). This 7T strategy paves the way to better identification of thalamic nuclei for neurosurgical planning and investigation of regional changes in neurological disorders.



**Corresponding author:** Thomas Tourdias MD, PhD Service de Neuroimagerie Diagnostique et Thérapeutique Université de Bordeaux, CHU de Bordeaux Place Amélie Raba Léon Bordeaux, France, 33076 cedex Phone:+33 (0)5 56 79 56 04 tourdias@stanford.edu; thomas.tourdias@chu-bordeaux.fr.
[1]Permanent address Service de Neuroimagerie Diagnostique et Thérapeutique Université de Bordeaux, CHU de Bordeaux Place Amélie Raba Léon Bordeaux, France, 33076 cedex
**Author contacts:** manojsar@stanford.edu ives@stanford.edu sujason@stanford.edu brutt@stanford.edu

**Keywords**

Thalamus; Thalamic nuclei; white matter nulled MPRAGE; Ultra High Field; 7T

## 1. INTRODUCTION

The thalamus is often described as a “relay organ” involved in a wide range of neurological functions including motor, sensory, integrative, and higher cortical functions. It also plays a significant role in other functions such as the regulation of sleep and wakefulness, memory, emotion, consciousness, awareness, and attention (Sherman, 2005). The thalamus is not a single structure but is composed of several functionally specific nuclei interlocked in a complex anatomy (Morel et al., 1997).

The ability to image the detailed internal structure of the thalamus *in vivo* is appealing for several clinical and research applications. First, it will open the way to direct anatomical targeting for planning of deep brain stimulation of multiple thalamic sub-regions (Lemaire et al., 2007). Better visualization of thalamic nuclei could improve the safety of new strategies such as focused ultrasound thalamotomy where neurophysiological recording cannot be used to correct potential errors due to atlas-based mis-targeting (Lipsman et al., 2013). Second, direct imaging of thalamic nuclei could enable the investigation of regional thalamic changes that could account for specific symptoms observed in psychiatric disorders (Coscia et al., 2009), Alzheimer's disease (Zarei et al., 2010), Parkinson's disease (McKeown et al., 2008), or multiple sclerosis (Minagar et al., 2013).

Delineation of the intra-thalamic nuclei has been proposed with various cluster-based image segmentation methods, where each voxel is assigned to a specific cluster (and in turn to a nucleus) based on feature similarity and spatial proximity. Notably, several diffusion tensor imaging (DTI)-based clustering techniques have been reported (Behrens et al., 2003; Jbabdi et al., 2009; Mang et al., 2012; Wiegell et al., 2003); however, these approaches suffer from the low spatial resolution of DTI images and the low fractional anisotropy within the thalamus, and are sensitive to user-defined parameters, decreasing the reproducibility of the results. Clustering using quantitative T1 and T2 relaxation times has also been suggested, but requires long scans (Deoni et al., 2005) and *a priori* knowledge of the relative positions of the nuclei (Deoni et al., 2007; Traynor et al., 2011). Furthermore, different clustering methods could yield inconsistent results (Traynor et al., 2011), a strong argument for direct anatomical visualization of the thalamic sub-structures.

Nevertheless, direct anatomical delineation of the sub-nuclei faces major challenges due to the low intrinsic intra-thalamic MR contrast obtained with standard T1-weighted or T2-weighted sequences and the small size of the sub-nuclei. Varying myelin concentration throughout the different sub-nuclei was observed histologically (Morel, 2007). Hence inversion recovery (IR) T1-weighted pulse sequences (Deichmann et al., 2000; Deichmann et al., 2004) where contrast is mostly dependent on the presence of myelin, could be particularly suitable for high resolution and high contrast 3D imaging of the thalamus. In line with this reasoning, modifications of the magnetization-prepared rapidly-acquired gradient echo (MPRAGE) sequence have been suggested to visualize some intra-thalamic structures (Bender et al., 2011; Sudhyadhom et al., 2009; Vassal et al., 2012). In particular, intra-thalamic T1 contrast seems to be enhanced through the use of different inversion times (TI) than commonly used, specifically to null either white matter (WM) (Sudhyadhom et al., 2009; Vassal et al., 2012) or grey matter (GM) (Bender et al., 2011; Magnotta et al., 2000). One disadvantage of this strategy is that TIs shorter than the standard anatomical MPRAGE sequence (Jack et al., 2008) decrease the signal-to-noise ratio (SNR), making it challenging

to achieve sufficient spatial resolution and contrast-to-noise ratio within the thalamus with standard (1.5T or 3T) scanners (Bender et al., 2011; Magnotta et al., 2000; Sudhyadhom et al., 2009; Vassal et al., 2012).

We hypothesized that ultra high field MRI (7T) could provide new solutions for visualizing thalamic anatomy by virtue of higher intrinsic SNR. Furthermore, due to increased T1 dispersion at high field (Rooney et al., 2007), higher contrast between tissues has been reported at 7T (Weiss et al., 2010) and subtle T1 differences may be enhanced at 7T (Bock et al., 2009) compared to 3T (Bock et al., 2013). The possibility of greater relaxation time differences between sub-nuclei at 7T could maximize subtle intra-thalamic contrast after proper sequence optimization, while the greater intrinsic SNR at 7T should allow imaging at sufficiently small voxel size to resolve the internal anatomic sub-structures of the thalamus.

In this paper, we present a step-by-step optimization of the 3D MPRAGE pulse sequence at 7T, which we have specifically optimized to visualize the intra-thalamic nuclei. We first measured the T1 values of the thalamus at 7T using a standard single-slice IR method. We then used these T1 values to simulate the MPRAGE signal behavior, and used these theoretical results to guide empirical optimization through imaging of volunteers to achieve the best trade-off between signal, contrast, and resolution for visualization of the thalamic nuclei. Finally, we used the optimized sequence to show the correspondence of the MR images to anatomy by comparison to a standard stereotactic atlas (Krauth et al., 2010; Morel et al., 1997), and demonstrate the consistency of the new imaging method.

## 2. METHODS and THEORY

### 2.1. T1 measurements

Deoni *et al.* (Deoni et al., 2005) showed significant differences in T1 between intra-thalamic nuclei, with values ranging from 700ms to 1400ms at 1.5T; however, there is no literature reporting T1 values in sub-regions of the thalamus at 7T. To understand and optimize the intra-thalamic signal and contrast, we first obtained T1 maps on a 7T whole body MRI scanner (GE Discovery MR950, GE Healthcare, Waukesha, WI) using a 32 receive-channel head coil (Nova Medical Inc, Wilmington, MA) on 5 volunteers (4 male/ 1 female, mean age=33 years old, range 30-35). An IR fast spin echo (IR-FSE) sequence was acquired from a single axial slice covering the long axis of the thalamus at the level of the Monroe foramens, and repeated using 5 TIs (50, 200, 600, 1500 and 4000ms). The other relevant parameters were as follow: ETL=8, TE=9ms, TR=5000ms, BW=15.6KHz, FOV=18cm × 18cm, matrix=192 × 192, slice thickness=1.5mm, NEX=2 averages, and total acquisition time for all 5 TIs =20.4 min. Inversion was performed using the hyperbolic secant adiabatic pulse supplied in the vendor software (duration=16ms, bandwidth=1.5kHz), with the slice-selection gradient amplitude set to zero and increased pulse amplitude to ensure adiabatic performance (peak B1 amplitude = 2.28 $\mu$T). Because of its adiabatic characteristics, this pulse inverted spins with minimal sensitivity to the B1 inhomogeneity associated with 7T imaging in human brain. To generate the T1 maps, the IR-FSE images were analyzed with a general 4-parameter model for mono-exponential IR with polarity-restoration, taking into account the finite TR and imperfect inversion, using freely available code (Barral et al., 2010) in Matlab (The Mathworks, Natick, MA, USA).

T1 values were measured on the maps within manually-identified regions of frontal WM, cortical GM (anterior insular cortex), and thalamus. For the thalamus, we measured T1 values within several sub-regions based on known anatomy, notably in the pulvinar and the mediodorsal nuclei (which show T1 values spanning the higher range of the intra-thalamic T1 distribution at 1.5T (Deoni et al., 2005)) and within the adjacent nuclei from the median and lateral groups (which show T1 values spanning the lower range of the intra-thalamic T1

distribution at 1.5T (Deoni et al., 2005)). The regions-of-interest (ROI) used for T1 measurement and then for sequence optimization are illustrated in Figure 1.

### 2.2. Theory and Simulations for sequence optimization

The MPRAGE pulse sequence consists of an inversion pulse followed by an inversion delay (TI), a readout sequence consisting of a train of N low-flip-angle (α) gradient echo (GE) readouts with a short repetition time (TR), and an additional relaxation delay (TD) before the next inversion. For each inversion pulse, all kz slice-encoding steps are acquired – typically with centric ordering – and the process is repeated for all ky phase encoding steps in a sequential manner. The total duration, or shot interval (TS), between successive inversion pulses is given by TS=TI+(N*TR)+TD. During the TI and TD intervals, the longitudinal magnetization freely relaxes with a time constant T1 toward the thermal equilibrium $M_0$, while during the readout phase, the magnetization is driven by the α pulse train toward a steady state with a time constant T1* (Deichmann et al., 2000); commonly this steady state is closely approached within a hundred α pulses (Deichmann et al., 2000; Mugler and Brookeman, 1990). There is also an overall steady state being reached after 2 to 3 TS intervals, that accounts for all three transient phases.

In order to characterize the magnetization evolution in the MPRAGE sequence, we modeled the k-space signal modulation in the slice-encoding direction in Matlab using the formalism proposed by Deichmann *et al* (Deichmann et al., 2000). We used T1 values from our measurements, along with proton density (ρ) values from the literature (Neeb et al., 2006), to model the signal of the WM, the GM, and adjacent intra-thalamic regions with T1 values in the lower and higher range of thalamic T1 (see above and Figure 1). The parameters used for the modeling are summarized in **Table 1**. The signal amplitude at the center of k-space (called S) was used in the SNR and SNR efficiency calculations. To account for receiver bandwidth (BW) and the number of kz steps (N), we calculated SNR as S/sqrt(BW*N) and to account for the total scan time we calculated SNR efficiency as S/sqrt(BW*N*TS). CNR and CNR efficiency were similarly defined, but used the relative signal difference between two tissues of interest. In order to characterize the blurring at interfaces, a synthetic phantom consisting of a circular region of thalamus (diameter ~18 pixels) with a smaller circular region of WM (diameter ~4 pixels) was used to generate 2D k-space and the signal modulation was applied along one of the dimensions to simulate blurring along the MPRAGE signal readout (kz). Line profiles through the center of the phantom were used to study the effect of α on blurring. This phantom was structurally and compositionally similar to small WM interfaces observed inside the thalamus.

### 2.3. In vivo experiments for sequence optimization

Seventeen MR sessions were conducted on healthy volunteers (12 male / 5 female, mean age 37.9 years old, range 30-57) to verify the simulations and to finely optimize the sequence on the 7T GE Discovery MR950. This empirical optimization guided by the simulations was important especially when there was not a single optimal theoretical value but rather tradeoff between signal, contrast and blur in this complex optimization problem. Written informed consent was obtained before the imaging sessions for all participating subjects and the study was approved by the Institutional Review Board of Stanford University.

Static magnetic field (B0) inhomogeneities and transmit and receive (B1+ and B1−) inhomogeneities are major challenges at 7T (Truong et al., 2006) and can easily overwhelm the expected subtle signal variations between thalamic nuclei. All exams began with a higher order shim procedure to optimize linear and second order shims based on a 3D field map acquired over the whole brain. Typical residual B0 field variations were about 20 Hz rms over the brain and did not cause any artifact or image degradation especially for the

thalamus, located in the center of the brain. To mitigate B1+ inhomogeneity and stabilize the inversion throughout the brain volume, a nonselective hyperbolic secant pulse optimized to be insensitive to B1 and B0 heterogeneity was used (Saranathan et al., 2013), with a peak B1+ amplitude that was at least three times higher than the adiabatic threshold. B1+ maps were obtained using the Bloch-Siegert shift method (Sacolick et al., 2010) to quantify the B1+ variations and to assess the discrepancy between the prescribed and the true flip angle in the area of the thalamus.

During the optimization procedure, the 3D MPRAGE images were acquired with multiple sets of parameters following the steps described below ("2.4. Strategy for sequence optimization") and the corresponding details will be found in the figure captions.

All images were anonymized and evaluated by an experienced neuroradiologist for their ability to depict intra-thalamic nuclei and to measure signal, contrast and blur within the thalamus. SNR was defined as $S_{tissue} / SD_{background}$, where S denotes signal intensity and SD the standard deviation. Care was taken to place the ROI for noise evaluation in air away from phase encoding and other artifacts and at the same place each time to minimize errors due to spatially varying noise characteristics produced by the ARC parallel imaging technique. The relative intra-thalamic contrast was defined between adjacent nuclei (labeled A and B) as $(S_{nucleus\ A} - S_{nucleus\ B}) / (S_{nucleus\ A} + S_{nucleus\ B})$. As an index of the blur within the thalamus, we focused on the mammillothalamic tract (MTT) on axial views, as it represents a small WM structure (1 to 2 mm) embedded within the GM of the ventral anterior nucleus (Morel et al., 1997). Any blur will induce changes in the signal of the MTT by mixing with the adjacent ventral anterior nucleus. Consequently, the signal intensity profile was plotted along a line passing through the MTT on axial views and the shape of the curve was used to quantify the blur. The contrast between the MTT and the adjacent ventral anterior nucleus was also used as a surrogate measure of the blur.

### 2.4. Strategy for sequence optimization

MPRAGE with nulling of either WM (Sudhyadhom et al., 2009; Vassal et al., 2012) or GM (Bender et al., 2011; Magnotta et al., 2000) has been reported as a potential solution to increase intra-thalamic contrast; therefore, we first investigated which regime would provide the best strategy at 7T. The signal was modeled as a function of TI to find the null points for WM and GM and to predict intra-thalamic signal and contrast for each regime. The simulated results were verified experimentally by acquiring MPRAGE images at each nulling regime. For comparison, standard T1-weighted MPRAGE images were also acquired following the recommended parameters for morphometric analyses (Jack et al., 2008), slightly adjusted for 7T.

Once the global optimal nulling regime was determined, we investigated the effect of the length and the distribution of each MPRAGE period, *i.e, (i)* TS, *(ii)* the readout (N*TR) and *(iii)* TI. We first investigated the impact of TS by simulating intra-thalamic SNR and SNR efficiency, as well as intra-thalamic contrast and contrast efficiency, over a range of TS from 2000ms to 9000ms obtained by varying TD with other parameters fixed or calculated to remain in the same regime. The results of the simulations were assessed experimentally by acquiring scans with various TS through varying TD at the predefined optimal regime. The impact of N and TR were simultaneously studied by simulating SNR and SNR efficiency at each TS for N from 160 to 220 together with varying BW (and indirectly TR) from 10KHz to 40KHz. For the predefined optimal parameters, the TI was further finely tuned experimentally around the global optimal regime. Finally, we simulated the impact of $\alpha$ on signal, contrast and blur by varying $\alpha$ from 3° to 15° in the simulations and by varying the prescribed $\alpha$ from 2° to 10° *in vivo*, with other parameters fixed. The different $\alpha$ values

between simulations and experiments account for the difference between the actual and prescribed α based on B1 maps.

### 2.5. Direct visualization of the thalamic sub-nuclei

A set of whole brain 3D high-quality anatomical images was acquired in a group of 6 volunteers (5 males / 1 female, mean age 31.2 years old, range 24-35) with the optimized MPRAGE parameters obtained from the above steps. The optimized images were first reformatted in orthogonal planes and visually compared to classical histological plates from the well-known multiarchitectonic, stereotactic Morel atlas (Morel et al., 1997). Then, 15 substructures were manually and independently outlined for all 6 subjects, using only image features visualized in the MPRAGE images, by a neuroradiologist trained on thalamic anatomy. Evaluation was done with the software package 3D-Slicer (Version 4.2.2-1; http://www.slicer.org/) using freehand spline drawing tools to build 3D vector-based model (VTK) of each structure. Using the Morel nomenclature the 15 substructures were: *(i)* from the medial group the mediodorsal nucleus (MD), center median nucleus (CM), habenular nucleus (Hb); *(ii)* from the posterior group the pulvinar (Pul), medial geniculate nucleus (MGN), lateral geniculate nucleus (LGN); *(iii)* from the lateral group the ventral posterior lateral nucleus (VPL), ventral lateral anterior nucleus (VLa), ventral lateral posterior nucleus (VLp), ventral anterior nucleus (VA); *(iv)* from the anterior group the anterior ventral nucleus (AV), lateral dorsal nucleus (LD); *(v)* and also the red nucleus (RN), mammillothalamic tract (MTT) and subthalamic nucleus (STh). The volumes of these structures and the intercommissural distance for each subject were measured. Each brain was then linearly transformed to Talairach space and scaled in 3D to compensate for brain size differences between individuals and the atlas using a method inspired from Chakravarty *et al* (Chakravarty et al., 2009). The scaling factor in x was equal to (atlas width of the thalamus / subject width of the thalamus); in y was equal to (atlas intercommissural distance / subject intercommissural distance); and in z was equal to (atlas height of the thalamus / subject height of the thalamus). The transformation matrix calculated by 3D-Slicer was applied to the 3D volumes of the substructures obtained from the raw images, and the 3D Talairach center of mass (COM) coordinates of each nucleus were computed using Python scripts in 3D-Slicer. The 3D Talairach COM coordinates of an electronic version of the Morel atlas provided in Talairach space (Krauth et al., 2010) were computed using the same method for comparison. The mean Euclidean distance between the MR-defined COM and the atlas-defined COM was calculated. Reproducibility of the MR-based delineation was assessed by repeating the outlining of the structures by the same trained rater a second time after a 3-week interval to avoid recall bias.

### 2.6. Statistical analysis

We used the non-parametric Mann-Whitney test to compare the intercommissural distance measured on the 6 volunteers scanned with the optimized protocol and the intercommissural distances of the brains used for the atlas (Krauth et al., 2010; Morel et al., 1997). The Mann-Whitney test was also used to compare the MR-defined and atlas-based thalamic volumes (Krauth et al., 2010). Intra-rater reliability was assessed by calculating the intraclass correlation coefficient (ICC) for the volumes of substructures measuring absolute agreement under a two-way random ANOVA model. Also, the difference between the COM of the substructures computed during the first and the second reading sessions was calculated. Analyses were performed with the R software package (version 3.0.0).

# 3. RESULTS

## 3.1. T1 measurements

We measured mean frontal WM T1 to be 1201ms ±36ms and mean cortical GM T1 (anterior insular cortex) to be 1962ms ±46ms. Within the thalamus, a large range of T1 values was observed, ranging from about 1250ms to 1800ms **(Figure 1 and supplemental table)**. The highest T1 values were measured in the posterior and medial thalamus [pulvinar (Pul) and mediodorsal (MD) nuclei respectively] while T1 values were lower in the more lateral and anterior nuclei. Interestingly, even within a large nucleus group such as the lateral group, a range of T1 values was also observed within subdivisions, which bodes well for using a strongly T1-weighted sequence such as MPRAGE to reveal intra-thalamic contrast.

The next steps of simulation and sequence optimization were conducted to maximize the signal and the contrast between T1 values of 1800ms as the higher range of values measured in the pulvinar (Pul) and mediodorsal (MD) nuclei, and T1 values of 1400ms as the range of value measured in the adjacent center median (CM) and ventral posterior lateral (VPL) nuclei, in our population.

## 3.2. Sequence optimization

We first explored TI values centered around the null points for the major tissue classes (cerebro-spinal fluid – CSF for standard T1 contrast, GM, and WM) with the goal of revealing thalamic anatomy. The plot of the simulated signal versus TI indicated the theoretical WM, GM and CSF nulling values for a given set of TS/TR/N/α **(Figure 2A)**. The plots of relative intra-thalamic and WM/thalamus contrast versus TI are shown in **Figure 2B**. These simulations predict that despite good SNR **(Figure 2A)**, the standard MPRAGE sequence using long TIs (TI=1200ms for TS=3700ms) to get classical T1-weighted images provides poor signal separation between thalamus and adjacent WM as well as poor intra-thalamic contrast **(Figure 2B)** which was confirmed by the absence of any visible internal structure *in vivo* **(Figure 3C)**. Using the WM null regime rather than the GM null regime should lead to *(i)* about 38% increase of maximal intra-thalamic signal **(Figure 2A)** and to *(ii)* the best contrast between the external regions of the thalamus (exhibiting the lower T1 values) and the adjacent WM of the internal capsule **(Figure 2B).** Both the WM null and GM null regimes are close to the peaks of intra-thalamic contrast but the WM null regime provides positive contrast (higher T1 resulting in higher signal) and we further expect the WM null regime to reveal thin myelin rich lamellae separating the thalamic nuclei (Jones, 1985) that should appear strongly hypointense at this WM null point **(Figure 2B)**. *In vivo* scans **(Figure 3)** revealed accurate nulling of the GM using the TI predicted by theory (= 1080ms for TS=5000ms) for a GM T1 of 1962ms; for WM, ideal nulling WM was achieved for a shorter TI than predicted (= 730ms for TS=5000ms), corresponding to a WM T1 of 1100ms instead of the measured 1201ms (see discussion for further explanation of this discrepancy). In line with the simulations, the WM null images provided far better visual delineation of the thalamus from the surrounding tissues compared to the GM null images **(Figure 3A and B)**, a good intra-thalamic contrast and thin hypointense boundaries between some nuclei **(Figure 3A)** providing the rationale to further study this regime.

Next, we demonstrated the effect of increasing TS, by increasing TD, on thalamic signal and contrast. The thalamic signal **(Figure 4A)** and contrast **(Supplemental Figure 1)** were predicted to increase continuously with TS but with much bigger effect on signal than on contrast; the signal being in turn the main factor to pick the optimum value. As TS affects the overall imaging time for the sequence, we considered efficiency to determine the optimum TS **(Figure 4B)**. Signal efficiency peaked for TS=6000ms indicating that up to this value, the effect of lengthening TS was stronger than signal averaging for increasing SNR.

Experimentally, the gain of imaging at longer TS effected through longer TD was demonstrated by improved visualization of small nuclei **(Figure 4D)**.

The length of the readout train (N*TR) was optimized simultaneously with TS and TI and had different impact at different TS. For the long TS (6000ms) needed to maximize the signal and the contrast **(Figures 4A, 4B and supplemental Figure 1)**, a long readout (high N, low BW resulting in long TR) was predicted to produce more SNR efficiency **(Figure 4C)**. The impact on contrast was very low **(Supplemental Figure 1).** At TS=6000ms with the longer readout train, TD was still long enough (~3950ms) to allow sufficient relaxation of the longitudinal magnetization prior to the next inversion pulse. We ran our scans at 85-90% of the maximum SNR efficiency by using N=200, sufficient to cover the whole brain, and BW=20 KHz to increase SNR while avoiding the chemical shift artifacts that occurred at lower BW.

Fine experimental tuning of TI around the WM nulling point for TS=6000ms was found to be useful to improve thalamic nuclei delineation, by finding the best tradeoff between signal and contrast. From the simulated signal evolution over TI **(Figure 2A and B)**, it appeared that, close to the WM nulling point, increasing TI should decrease thalamic signal while improving intra-thalamic contrast; decreasing TI should have the opposite effect. This was particularly relevant to distinguishing subtle thalamic divisions *in vivo* as illustrated in **Figure 5**. Overall, the TS/TI=6000ms/670ms combination was found to be optimal for revealing intra-thalamic structures. Longer TI (TS/TI=6000ms/720ms) resulted in more complete WM suppression but also in important signal loss of lateral nuclei with T1 values closer to WM, thus obscuring accurate segmentation. On the other hand, with a shorter TI (TS/TI=6000ms/620ms), thin internuclear borders believed to correspond to thin myelin layers separating individual nuclei were progressively lost.

Finally, the optimal $\alpha$ was defined by finding the best tradeoff between signal and blur. Thalamic signal increased linearly with $\alpha$ as expected from the MPRAGE equation where signal is proportional to $\sin(\alpha)$ **(Figure 6C)**. At the WM null TI, the magnetization curve for the thalamus starts with negative values and changes sign during the acquisition of the phase encoding steps resulting in a more distorted point spread function than the standard MPRAGE, where the magnetization is positive throughout (data not shown). In simulations, the resulting blur in the 1D phantom was observed to increase rapidly with $\alpha$ **(Figure 6A)** and was suspected to result in progressive fading of small intra-thalamic structures. This effect appears predominantly in the slice encoding direction (antero-posterior for our coronal acquisition), and resulted in the visualization of small WM tracts, such as the mammillothalamic tract and the small internuclear borders, being progressively lost at higher $\alpha$ **(Figures 6B and 6D)**. A small prescribed flip angle of $\alpha$ =4° was chosen to allow 3D visualization with minimal blurring while maintaining sufficient signal **(Figure 6C)**. This prescribed $\alpha$ of 4° corresponds to an actual $\alpha$ of 5°-6° within the thalamus when accounting for the central B1 “hotspot” at 7T.

### 3.3. Direct visualization of the thalamic sub-nuclei

Based on the above stepwise strategy for optimization, we chose a final set of optimum parameters for visualizing thalamic anatomy as follows: TS=6000ms, TI=670ms, N=200, BW=20KHz, TR/TE=6.9ms/3.0ms, $\alpha$=4°, 1×1×1mm$^3$ acquisition resolution (0.7×0.7×0.5 mm$^3$ reconstructed voxel size) and centric 1D kz ordering. The protocol was used without parallel imaging (scan time=16. 2 min) but can be used with 1D parallel imaging acceleration (with acceleration factor in the range of 2-3) without significant alteration in imaging characteristics with the exception of signal to noise ratio (scan time ranging from 5.5min to 9 min).

The 6 volunteers scanned with this protocol had an average intercommissural distance of 28.3mm (range 26-30.5mm) that tended to be larger than the average intercommissural distance of the 5 brains used for the atlas (25.4mm; range 23-29mm; p=0.06). We found a mean thalamic volume over the 6 volunteers of 6571mm$^3$ (range 5887-7211mm$^3$); this was statistically larger than the mean thalamic volume from the atlas (5253mm$^3$; p=0.03).

Representative orthogonal slices obtained in 3 volunteers illustrate the consistent contrast across individuals **(Figure 7)**. Two characteristics were useful to delineate the nuclei on these MR images: *(i)* signal intensity variations between adjacent nuclei as expected from the quantitative T1 data shown in **Figure 1**; *(ii)* thin bands of reduced signal surrounding and separating many adjacent nuclei with otherwise close signal intensity. Visual comparison with the atlas showed that such contrast variation and thin hypointense boundaries corresponded well with known anatomical structures of the thalamus, although slight differences between the MR-defined nuclei and the atlas were also noticeable.

The above-mentioned characteristics (contrast variation and thin hypointense bands) allowed a 3D delineation of 15 structures in each volunteer. The COM coordinates showed tight clusters close to the atlas-based COM coordinates, with a mean Euclidean distance discrepancy from the atlas-based COMs of 2.67mm (±1.02mm) **(Figure 8)**. As expected the smaller nuclei (such as LD) showed a slightly wider spread. This quantification provided more evidence that the sequence showed contrast allowing the recognition of known anatomical/histological structures.

The nuclei were outlined from MR images with an overall excellent reproducibility. The ICC for the volumes of substructures was measured at 0.997 (95% confidence interval 0.996 < ICC < 0.998). The mean Euclidean distance discrepancy between corresponding COMs found at first versus second readings was very small (0.69mm ±0.38mm) and in fact smaller than the voxel dimension.

## 4. DISCUSSION

We have combined theoretical simulations and empirical optimization to obtain a WM-nulled version of MPRAGE at 7T and we have shown its ability to reveal detailed intra-thalamic structures in individual subjects. This opens the door to new solutions for planning of deep brain stimulation and other targeted deep brain therapeutic strategies, and for investigation of regional thalamic changes in several neurological disorders.

Compared to existing methods aimed at targeting thalamic anatomy, the solution presented in this paper offers direct anatomical images obtained in a clinically acceptable imaging time and without post processing. The full 3D coverage with multiplanar reconstruction revealed small substructures and subdivisions not clearly discriminated otherwise. Clustering methods using DTI-based feature similarities (Behrens et al., 2003; Jbabdi et al., 2009; Mang et al., 2012; Wiegell et al., 2003) are attractive because they could be independent of the manual delineation used here. Nevertheless, we were able to identify small thalamic sub-regions not detectable with DTI-based clustering and a single DTI-based cluster may represent the sum of smaller histological subdivisions that cannot be assessed *in vivo* with that technique. Based on the dispersion of T1 values shown in Figure 1 and recent solutions for fast 3D T1 mapping at 7T (Liu et al., 2011), we could consider coupling our high-quality anatomical data with T1-based segmentation algorithms in the future to help find nuclear boundaries semi-automatically. Other anatomical methods have been suggested to enhance thalamic contrast but were usually only able to distinguish the limited number of nuclei generating the highest intrinsic contrast (Gringel et al., 2009; Kanowski et al., 2010). Here, in addition to the enhanced contrast, we also showed thin bands reminiscent of inter-nuclear

borders seen on histological sections (Jones, 1985), compatible with the presence of thin myelin layers or sheaths (signal suppressed in our WM null regime) separating individual nuclei. These thin bands, although not easily identifiable on all contiguous slices, were useful to differentiate adjacent nuclei with otherwise close signal. This observation was first reported by Deoni *et al*. (Deoni et al., 2005) at 1.5T with multi-average scans over a clinically unrealistic 13 hours. Our optimization procedure and the intrinsic higher SNR of the 7T system have achieved the critical conditions to distinguish these structures in a clinically practical scan time. The concept of WM-nulled MPRAGE for thalamic imaging has already appeared in the literature at 1.5T (Vassal et al., 2012) and 3T (Sudhyadhom et al., 2009); however, the lower SNR at these field strengths probably explains why the thin boundaries have not been reported using this method in the past.

Three main issues specific to the WM-nulled regime implementation at 7T were addressed during our experiments. First, the theoretical prediction of the nulling point TI based on the MPRAGE signal equation required accurate T1 values, and our T1 measurements were in good agreement with other published values at 7T (Rooney et al., 2007). Nevertheless, for a WM T1 of 1201ms, the predicted WM-null point TI of 800ms (for TS=5000ms) did not perfectly null the WM, while a nulling point TI of 730ms, corresponding to a T1 of 1100ms, allowed more effective WM suppression in our experiments. No such difference was observed for GM, where the predicted matched the experimental TI null (= 1080ms). Additional analysis of our T1 data (not shown) revealed that multi-exponential T1 relaxation, not accounted for in our mono-exponential T1 measurements or in the MPRAGE model (Deichmann et al., 2000), could explain this effect. Two possible mechanisms for multi-exponential relaxation are present in brain tissue: magnetization transfer (MT) effects (Dortch et al., 2013; Henkelman et al., 2001; Prantner et al., 2008) and multi-compartment water relaxation (Labadie et al., 2013; MacKay et al., 2006). Both effects result in more complex non-mono-exponential relaxation following inversion-preparation, and could explain this observation. The MT mechanism of cross-relaxation and partial saturation of the macromolecular pool can be shown to reduce the effective WM-nulling TI. Multi-compartment water relaxation could also contribute to this effect in the same direction. The greater MT effect and fast-relaxing water fraction in WM compared to GM (both related to presence of myelin) are consistent with the larger shift between predicted and actual nulling TI values in WM versus GM. Accurate prediction of the nulling TI would require description of MPRAGE signal behavior that includes both of these effects, which is beyond the scope of this work. Scaling back the WM T1 by about 100ms was sufficient to empirically compensate for this effect, and resulted in correct predictions of the nulling TI value using our simulations. Furthermore, we found that fine experimental tuning of TI below the effective nulling point helped significantly to increase visualization of thalamic nuclei; therefore, an exact prediction of the nulling TI value may not be necessary.

Second, the shorter WM-nulling TI used here results in lower thalamic SNR compared to standard CSF-nulled MPRAGE if no additional post-readout delay (*i.e.* longer TD) is provided for recovery. We have demonstrated the benefit of lengthening TS over averaging to improve the signal and the contrast, in agreement with recent strategies to enhance T1 contrast within the cortex (Bock et al., 2013). Because longer TS increases scan time, acceleration is important, and in our study we exploited the better performance of parallel imaging techniques at ultra-high field (Wiesinger et al., 2004). We are currently developing versions of MPRAGE with two-dimensional (ky-kz) k-space ordering along the $\alpha$ pulse train to speed up the acquisition with minimal image degradation thanks to the better performance of 2D parallel imaging compared to 1D acceleration achievable with the standard centric ordering.

Third, the WM-nulled regime requires dealing with magnetization curves that start with negative values and change sign during the acquisition, resulting in a distorted point spread functions and accentuating the MPRAGE-related blur effect. We have shown in this study that α has a major effect on blur and that lower α was required to mitigate this effect and to achieve non-blurred 3D reconstructions. 3D images were very useful for anatomical recognition of the complex thalamic anatomy where different planes were preferred depending on the nucleus being analyzed. Given the higher SNR available at higher field, small α can advantageously be used at 7T to mitigate the blur while maintaining sufficient SNR. Some authors have suggested using k-space filtering to compensate the blur in classic MPRAGE (Deichmann et al., 2000). In this study, we preferred not to use such a compensating filter given the presence of zero crossings along our k-space signal modulations, and to avoid the elevated noise level inherent to such spatial filtering. Given the long TS and small α used here, the sequence had very low SAR, making this an easily implementable sequence at 7T, where SAR is often a tough constraint for other sequences.

Some remaining questions and unresolved problems need to be discussed. First, objectively assessing the accuracy of the MR outlines is difficult due to the lack of an absolute subject-specific gold standard. Thalamic atlases do not capture inter-individual variability and this likely explains our observation of imperfect correspondence between the MR- and atlas-based nuclei COM locations, even after differential linear scaling in all three orthogonal directions in an attempt to compensate for the overall thalamus size between the atlas and a given individual (this compensation being necessary to account for individual brain size differences and for the fact that the atlas thalamus size is reduced compared to the *in vivo* size because of shrinkage induced by the fixation process). A more complex atlas-to-MR non-linear registration might have better compensated for the inter-individual variability, and could have provided a better reference comparison. This procedure is beyond the scope of this paper and for this initial study we favored the clinically-relevant linear Talairach space registration. To assess the accuracy of the MR-defined structures more definitively, a comparison of the segmentation results with electrophysiological recordings made during surgery could be considered for the nuclei typically targeted during deep brain stimulation. Alternatively, MRI data obtained from a post mortem sample and subsequent histology could also establish the validity of the MR-definition of the intra-thalamic nuclear boundaries but would require a re-optimization of sequence parameters for fixed tissue. Second, our approach is purely based on T1 contrast. Other T1-weighted methods such as inversion-recovery turbo spin echo (IR-TSE) could be considered but are often associated with SAR above regulatory limits at 7T. Tuning the MP2RAGE sequence to get WM null contrast close to our optimization could be possible (Tanner et al., 2012) and could be of benefit in making quantitative T1 maps possible (Marques et al., 2010). The SNR efficiency of this strategy would need to be evaluated compared to MPRAGE optimization shown here. Furthermore, other sources of contrast could be added in the future to improve thalamic segmentation. Recent papers have shown the benefits of 7T susceptibility weighted imaging (Abosch et al., 2010) and particularly quantitative susceptibility mapping, QSM (Deistung et al., 2013) to reveal some thalamic anatomy. QSM methods nevertheless require complicated image acquisitions (with the head tilted in 3 different positions) and sophisticated post-processing method (Deistung et al., 2013) as opposed to the straightforward reconstruction of WM null MPRAGE images. Future work should investigate a comparison or a combination of our WM null MPRAGE and QSM approaches that could be relevant to identifying the T1/T2* signature of each thalamic nucleus – this could aid in automatic segmentation efforts. The ability to delineate thalamic anatomy with susceptibility-based contrast could be massively affected by iron content that is known to increase with age or pathological condition (Zecca et al., 2004). Although our T1-weighted approach is probably less sensitive to the variation of iron, iron content could still be a contributing factor to our

image contrast. Future work will be needed to understand how iron content may affect our ability to separate thalamic nuclei in older subjects or in pathological conditions.

## 5. CONCLUSION

In conclusion, by optimizing WM-nulled MPRAGE at 7T we have provided a strategy allowing direct anatomical visualization of thalamic sub-structures that are usually not clearly discriminated, paving the way for new clinical and research applications. Our method could have a strong impact on planning of deep brain stimulation procedures, and is worth evaluating in patients. Furthermore, by covering the whole brain and providing a strong contrast between WM and cortical GM, we expect that the method could become of great value in a number of applications where both the thalamus and cortical structures have to be well identified, such as in multiple sclerosis where there is a growing interest in visualizing both thalamic (Minagar et al., 2013) and cortical inflammatory lesions (Calabrese et al., 2010).

## Supplementary Material

Refer to Web version on PubMed Central for supplementary material.

## Acknowledgments

We acknowledge grant support from NIH grant P41 EB015891-19 and from GE Healthcare. T. Tourdias received financial support from ARSEP Foundation (Fondation pour l'aide à la recherche sur la Sclérose en Plaques); CHU de Bordeaux, Fondation Université de Bordeaux and Translational Research and Advanced Imaging Laboratory (TRAIL) program – France; Institut Servier; and France-Stanford Center for Interdisciplinary studies.

## ABRREVIATIONS

| | |
|---|---|
| **AV** | Anterior ventral nucleus |
| **CM** | Center median nucleus |
| **CNR** | Contrast-to-noise ratio |
| **COM** | Center of mass |
| **CSF** | Cerebro-spinal fluid |
| **GM** | Grey matter |
| **Hb** | Habenular nucleus |
| **ICC** | Intraclass correlation coefficient |
| **LD** | Lateral dorsal nucleus |
| **LGN** | Lateral geniculate nucleus |
| **MD** | Mediodorsal nucleus |
| **MGN** | Medial geniculate nucleus |
| **MPRAGE sequence** | Magnetization-prepared rapidly-acquired gradient echo sequence |
| **MTT** | Mammillothalamic tract |
| **Pul** | Pulvinar |
| **RN** | Red nucleus |
| **ROI** | Region-of-interest |

| | |
|---|---|
| **SNR** | Signal-to-noise ratio |
| **Sth** | Subthalamic nucleus |
| **TD** | Delay time |
| **TI** | Inversion time |
| **TS** | Shot interval time |
| **VA** | Ventral anterior nucleus |
| **VLa** | Ventral lateral anterior nucleus |
| **VLp** | Ventral lateral posterior nucleus |
| **VPL** | Ventral posterior lateral nucleus |
| **WM** | White matter |

## REFERENCES


Abosch A, Yacoub E, Ugurbil K, Harel N. An assessment of current brain targets for deep brain stimulation surgery with susceptibility-weighted imaging at 7 tesla. Neurosurgery. 2010; 67:1745–1756. discussion 1756. [PubMed: 21107206]

Barral JK, Gudmundson E, Stikov N, Etezadi-Amoli M, Stoica P, Nishimura DG. A robust methodology for in vivo T1 mapping. Magnetic Resonance in Medicine. 2010; 64:1057–1067. [PubMed: 20564597]

Behrens TE, Johansen-Berg H, Woolrich MW, Smith SM, Wheeler-Kingshott CA, Boulby PA, Barker GJ, Sillery EL, Sheehan K, Ciccarelli O, Thompson AJ, Brady JM, Matthews PM. Non-invasive mapping of connections between human thalamus and cortex using diffusion imaging. Nat Neurosci. 2003; 6:750–757. [PubMed: 12808459]

Bender B, Manz C, Korn A, Nagele T, Klose U. Optimized 3D magnetization-prepared rapid acquisition of gradient echo: identification of thalamus substructures at 3T. AJNR Am J Neuroradiol. 2011; 32:2110–2115. [PubMed: 21979493]

Bock NA, Hashim E, Janik R, Konyer NB, Weiss M, Stanisz GJ, Turner R, Geyer S. Optimizing T1-weighted imaging of cortical myelin content at 3.0 T. Neuroimage. 2013; 65:1–12. [PubMed: 23036446]

Bock NA, Kocharyan A, Liu JV, Silva AC. Visualizing the entire cortical myelination pattern in marmosets with magnetic resonance imaging. J Neurosci Methods. 2009; 185:15–22. [PubMed: 19737577]

Calabrese M, Filippi M, Gallo P. Cortical lesions in multiple sclerosis. Nat Rev Neurol. 2010; 6:438–444. [PubMed: 20625376]

Chakravarty MM, Sadikot AF, Germann J, Hellier P, Bertrand G, Collins DL. Comparison of piece-wise linear, linear, and nonlinear atlas-to-patient warping techniques: analysis of the labeling of subcortical nuclei for functional neurosurgical applications. Hum Brain Mapp. 2009; 30:3574–3595. [PubMed: 19387981]

Coscia DM, Narr KL, Robinson DG, Hamilton LS, Sevy S, Burdick KE, Gunduz-Bruce H, McCormack J, Bilder RM, Szeszko PR. Volumetric and shape analysis of the thalamus in first-episode schizophrenia. Hum Brain Mapp. 2009; 30:1236–1245. [PubMed: 18570200]

Deichmann R, Good CD, Josephs O, Ashburner J, Turner R. Optimization of 3-D MP-RAGE sequences for structural brain imaging. Neuroimage. 2000; 12:112–127. [PubMed: 10875908]

Deichmann R, Schwarzbauer C, Turner R. Optimisation of the 3D MDEFT sequence for anatomical brain imaging: technical implications at 1.5 and 3 T. Neuroimage. 2004; 21:757–767. [PubMed: 14980579]

Deistung A, Schafer A, Schweser F, Biedermann U, Turner R, Reichenbach JR. Toward in vivo histology: a comparison of quantitative susceptibility mapping (QSM) with magnitude-, phase-,

and R2*-imaging at ultra-high magnetic field strength. Neuroimage. 2013; 65:299–314. [PubMed: 23036448]

Deoni SC, Josseau MJ, Rutt BK, Peters TM. Visualization of thalamic nuclei on high resolution, multi-averaged T1 and T2 maps acquired at 1.5 T. Hum Brain Mapp. 2005; 25:353–359. [PubMed: 15852386]

Deoni SC, Rutt BK, Parrent AG, Peters TM. Segmentation of thalamic nuclei using a modified k-means clustering algorithm and high-resolution quantitative magnetic resonance imaging at 1.5 T. Neuroimage. 2007; 34:117–126. [PubMed: 17070073]

Dortch RD, Moore J, Li K, Jankiewicz M, Gochberg DF, Hirtle JA, Gore JC, Smith SA. Quantitative magnetization transfer imaging of human brain at 7 T. Neuroimage. 2013; 64:640–649. [PubMed: 22940589]

Gringel T, Schulz-Schaeffer W, Elolf E, Frolich A, Dechent P, Helms G. Optimized high-resolution mapping of magnetization transfer (MT) at 3 Tesla for direct visualization of substructures of the human thalamus in clinically feasible measurement time. J Magn Reson Imaging. 2009; 29:1285–1292. [PubMed: 19472385]

Henkelman RM, Stanisz GJ, Graham SJ. Magnetization transfer in MRI: A review. NMR in Biomedicine. 2001; 14:57–64. [PubMed: 11320533]

Jack CR Jr. Bernstein MA, Fox NC, Thompson P, Alexander G, Harvey D, Borowski B, Britson PJ, J LW, Ward C, Dale AM, Felmlee JP, Gunter JL, Hill DL, Killiany R, Schuff N, Fox-Bosetti S, Lin C, Studholme C, DeCarli CS, Krueger G, Ward HA, Metzger GJ, Scott KT, Mallozzi R, Blezek D, Levy J, Debbins JP, Fleisher AS, Albert M, Green R, Bartzokis G, Glover G, Mugler J, Weiner MW. The Alzheimer's Disease Neuroimaging Initiative (ADNI): MRI methods. J Magn Reson Imaging. 2008; 27:685–691. [PubMed: 18302232]

Jbabdi S, Woolrich MW, Behrens TE. Multiple-subjects connectivity-based parcellation using hierarchical Dirichlet process mixture models. Neuroimage. 2009; 44:373–384. [PubMed: 18845262]

Jones, EG. The thalamus. Plenum Press; New York: 1985.

Kanowski M, Voges J, Tempelmann C. Delineation of the nucleus centre median by proton density weighted magnetic resonance imaging at 3 T. Neurosurgery. 2010; 66:E121–123. discussion E123. [PubMed: 20173580]

Krauth A, Blanc R, Poveda A, Jeanmonod D, Morel A, Szekely G. A mean three-dimensional atlas of the human thalamus: generation from multiple histological data. Neuroimage. 2010; 49:2053–2062. [PubMed: 19853042]

Labadie C, Lee JH, Rooney WD, Jarchow S, Aubert-Frecon M, Springer CS Jr. Moller HE. Myelin water mapping by spatially regularized longitudinal relaxographic imaging at high magnetic fields. Magnetic Resonance in Medicine. 2013

Lemaire JJ, Coste J, Ouchchane L, Caire F, Nuti C, Derost P, Cristini V, Gabrillargues J, Hemm S, Durif F, Chazal J. Brain mapping in stereotactic surgery: a brief overview from the probabilistic targeting to the patient-based anatomic mapping. Neuroimage. 2007; 37(Suppl 1):S109–115. [PubMed: 17644002]

Lipsman N, Schwartz ML, Huang Y, Lee L, Sankar T, Chapman M, Hynynen K, Lozano AM. MR-guided focused ultrasound thalamotomy for essential tremor: a proof-of-concept study. Lancet Neurol. 2013; 12:462–468. [PubMed: 23523144]

Liu JV, Bock NA, Silva AC. Rapid high-resolution three-dimensional mapping of T1 and age-dependent variations in the non-human primate brain using magnetization-prepared rapid gradient-echo (MPRAGE) sequence. Neuroimage. 2011; 56:1154–1163. [PubMed: 21376814]

MacKay A, Laule C, Vavasour I, Bjarnason T, Kolind S, Madler B. Insights into brain microstructure from the T2 distribution. Magnetic Resonance Imaging. 2006; 24:515–525. [PubMed: 16677958]

Magnotta VA, Gold S, Andreasen NC, Ehrhardt JC, Yuh WT. Visualization of subthalamic nuclei with cortex attenuated inversion recovery MR imaging. Neuroimage. 2000; 11:341–346. [PubMed: 10725190]

Mang SC, Busza A, Reiterer S, Grodd W, Klose AU. Thalamus segmentation based on the local diffusion direction: a group study. Magn Reson Med. 2012; 67:118–126. [PubMed: 21656553]

Marques JP, Kober T, Krueger G, van der Zwaag W, Van de Moortele PF, Gruetter R. MP2RAGE, a self bias-field corrected sequence for improved segmentation and T1-mapping at high field. Neuroimage. 2010; 49:1271–1281. [PubMed: 19819338]

McKeown MJ, Uthama A, Abugharbieh R, Palmer S, Lewis M, Huang X. Shape (but not volume) changes in the thalami in Parkinson disease. BMC Neurol. 2008; 8:8. [PubMed: 18412976]

Minagar A, Barnett MH, Benedict RH, Pelletier D, Pirko I, Sahraian MA, Frohman E, Zivadinov R. The thalamus and multiple sclerosis: Modern views on pathologic, imaging, and clinical aspects. Neurology. 2013; 80:210–219. [PubMed: 23296131]

Morel A. Stereotactic atlas of the human thalamus and basal ganglia. Informa Healthcare. 2007:13–53.

Morel A, Magnin M, Jeanmonod D. Multiarchitectonic and stereotactic atlas of the human thalamus. J Comp Neurol. 1997; 387:588–630. [PubMed: 9373015]

Mugler JP 3rd, Brookeman JR. Three-dimensional magnetization-prepared rapid gradient-echo imaging (3D MP RAGE). Magn Reson Med. 1990; 15:152–157. [PubMed: 2374495]

Neeb H, Zilles K, Shah NJ. A new method for fast quantitative mapping of absolute water content in vivo. Neuroimage. 2006; 31:1156–1168. [PubMed: 16650780]

Prantner AM, Bretthorst GL, Neil JJ, Garbow JR, Ackerman JJ. Magnetization transfer induced biexponential longitudinal relaxation. Magn Reson Med. 2008; 60:555–563. [PubMed: 18759367]

Rooney WD, Johnson G, Li X, Cohen ER, Kim SG, Ugurbil K, Springer CS Jr. Magnetic field and tissue dependencies of human brain longitudinal 1H2O relaxation in vivo. Magn Reson Med. 2007; 57:308–318. [PubMed: 17260370]

Sacolick LI, Wiesinger F, Hancu I, Vogel MW. B1 mapping by Bloch-Siegert shift. Magn Reson Med. 2010; 63:1315–1322. [PubMed: 20432302]

Saranathan, M.; Tourdias, T.; Zeineh, M.; Kerr, A.; Berstein, J.; Kerchner, GA.; Rutt, B. Optimization of Cube-FLAIR 3D FSE Imaging at 7T.. Proceedings of the ISMRM; Salt Lack City. 2013; 2013. p. 248

Sherman SM. Thalamic relays and cortical functioning. Prog Brain Res. 2005; 149:107–126. [PubMed: 16226580]

Sudhyadhom A, Haq IU, Foote KD, Okun MS, Bova FJ. A high resolution and high contrast MRI for differentiation of subcortical structures for DBS targeting: the Fast Gray Matter Acquisition T1 Inversion Recovery (FGATIR). Neuroimage. 2009; 47(Suppl 2):T44–52. [PubMed: 19362595]

Tanner M, Gambarota G, Kober T, Krueger G, Erritzoe D, Marques JP, Newbould R. Fluid and white matter suppression with the MP2RAGE sequence. J Magn Reson Imaging. 2012; 35:1063–1070. [PubMed: 22170818]

Traynor CR, Barker GJ, Crum WR, Williams SC, Richardson MP. Segmentation of the thalamus in MRI based on T1 and T2. Neuroimage. 2011; 56:939–950. [PubMed: 21310246]

Truong TK, Chakeres DW, Beversdorf DQ, Scharre DW, Schmalbrock P. Effects of static and radiofrequency magnetic field inhomogeneity in ultra-high field magnetic resonance imaging. Magn Reson Imaging. 2006; 24:103–112. [PubMed: 16455399]

Vassal F, Coste J, Derost P, Mendes V, Gabrillargues J, Nuti C, Durif F, Lemaire JJ. Direct stereotactic targeting of the ventrointermediate nucleus of the thalamus based on anatomic 1.5-T MRI mapping with a white matter attenuated inversion recovery (WAIR) sequence. Brain Stimul. 2012; 5:625–633. [PubMed: 22405744]

Volz S, Noth U, Jurcoane A, Ziemann U, Hattingen E, Deichmann R. Quantitative proton density mapping: correcting the receiver sensitivity bias via pseudo proton densities. Neuroimage. 2012; 63:540–552. [PubMed: 22796988]

Weiss, M.; Geyer, S.; Lohmann, G.; Trampel, R.; Turner, R. Longitudinal relaxation time T1 as a guide to in-vivo myeloarchitecture.. Proceedings of the 16th Annual meeting of the Organization for Human Brain Mapping; 2010. p. 134

Wiegell MR, Tuch DS, Larsson HB, Wedeen VJ. Automatic segmentation of thalamic nuclei from diffusion tensor magnetic resonance imaging. Neuroimage. 2003; 19:391–401. [PubMed: 12814588]

Wiesinger F, Van de Moortele PF, Adriany G, De Zanche N, Ugurbil K, Pruessmann KP. Parallel imaging performance as a function of field strength--an experimental investigation using electrodynamic scaling. Magn Reson Med. 2004; 52:953–964. [PubMed: 15508167]

Zarei M, Patenaude B, Damoiseaux J, Morgese C, Smith S, Matthews PM, Barkhof F, Rombouts SA, Sanz-Arigita E, Jenkinson M. Combining shape and connectivity analysis: an MRI study of thalamic degeneration in Alzheimer's disease. Neuroimage. 2010; 49:1–8. [PubMed: 19744568]

Zecca L, Youdim MB, Riederer P, Connor JR, Crichton RR. Iron, brain ageing and neurodegenerative disorders. Nat Rev Neurosci. 2004; 5:863–873. [PubMed: 15496864]

## Highlights

- We optimized the MPRAGE sequence at 7T to enhance intra-thalamic T1 differences.
- An inversion time that nearly nulls white matter enhances thalamus contrast.
- In vivo 7T delineation of thalamic nuclei was reproducible and matched the atlas.
- 7T MPRAGE could improve surgical planning and studies of regional thalamic changes.

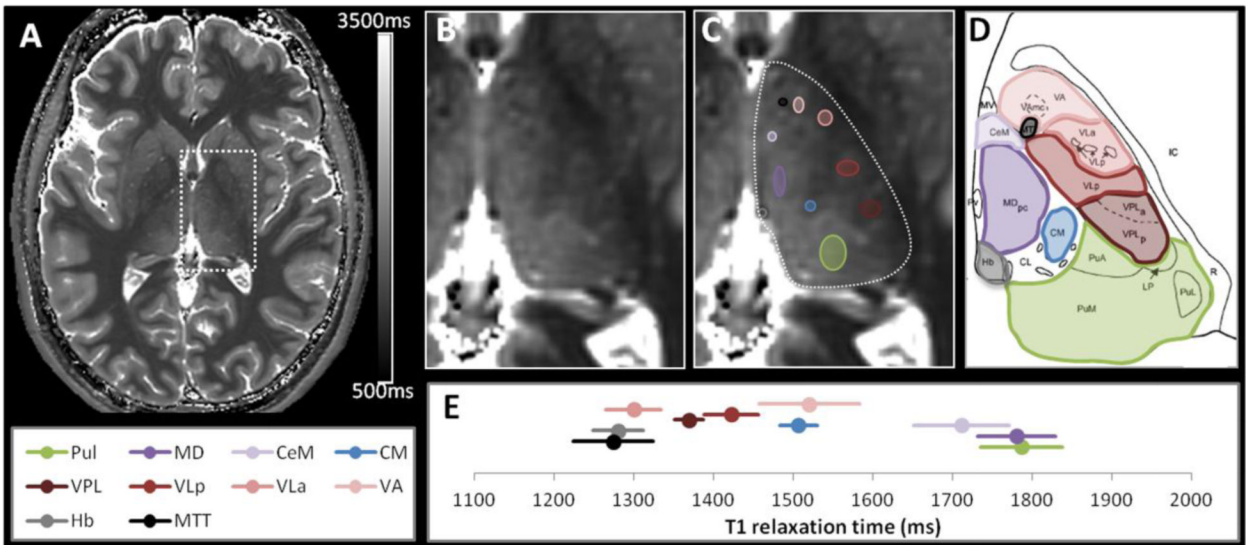


**Figure 1. T1 map and locations of the intra-thalamic regions of interest (ROI)**

A representative T1 map is shown **(A)** with an enlarged view of the left thalamus without **(B)** and with regions-of-interest (ROI) **(C)**. The corresponding plate of the Morel atlas (Morel et al., 1997) is shown for anatomic correspondence **(D)** (abbreviations as described in Methods). The mean T1 values and their corresponding across-subject standard deviations for the 5 volunteers are plotted in **(E, see also supplemental table)**. The colors of the ROI and of the segments on the plot match the colors used on the atlas plate.

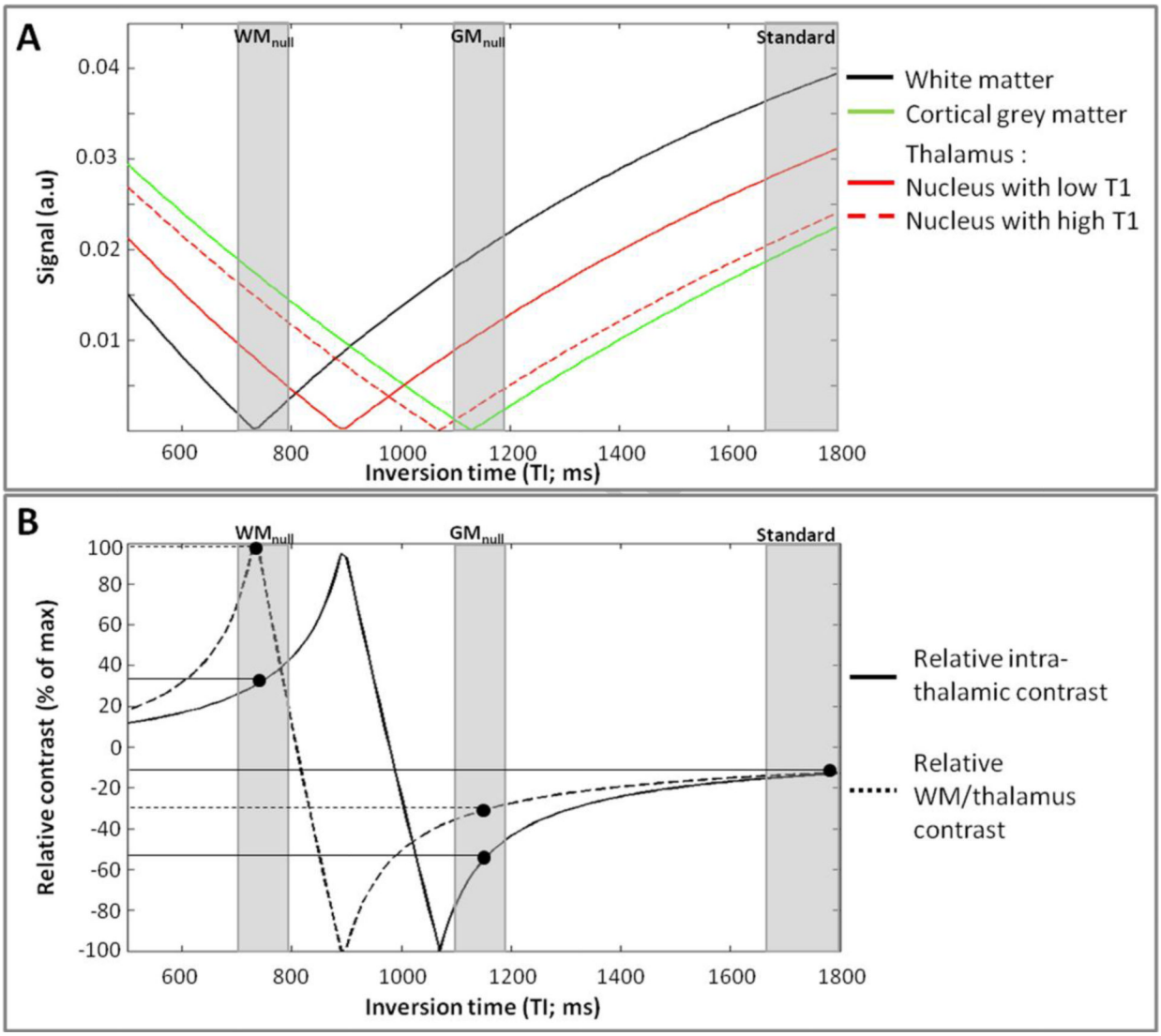


**Figure 2. Global regime of contrast - Simulations**

The signal intensity was simulated as a function of TI **(A)** with the other MR parameters as described for *in vivo* experiments in **Figure 3** and with the T1/PD values as described in Results (T1 measurements) and **Table 1**. The corresponding intra-thalamic relative contrast and the relative contrast between the external thalamus (exhibiting the lower T1 values) and the surrounding WM are shown in **(B)**. The contrast between structures A and B was defined as (A-B)/(A+B) rather than (A-B)/A to avoid divide-by-zero effects.

From these simulations, the standard MPRAGE (close to the CSF null regime) provides good signal but poor contrast within the thalamus and between the thalamus and the surrounding WM. The WM null regime yields about 38% increase of the maximum intra-thalamic signal compared to the GM null regime and the best contrast between the external thalamus and the surrounding WM while staying close to one of the peaks for intra-thalamic contrast.

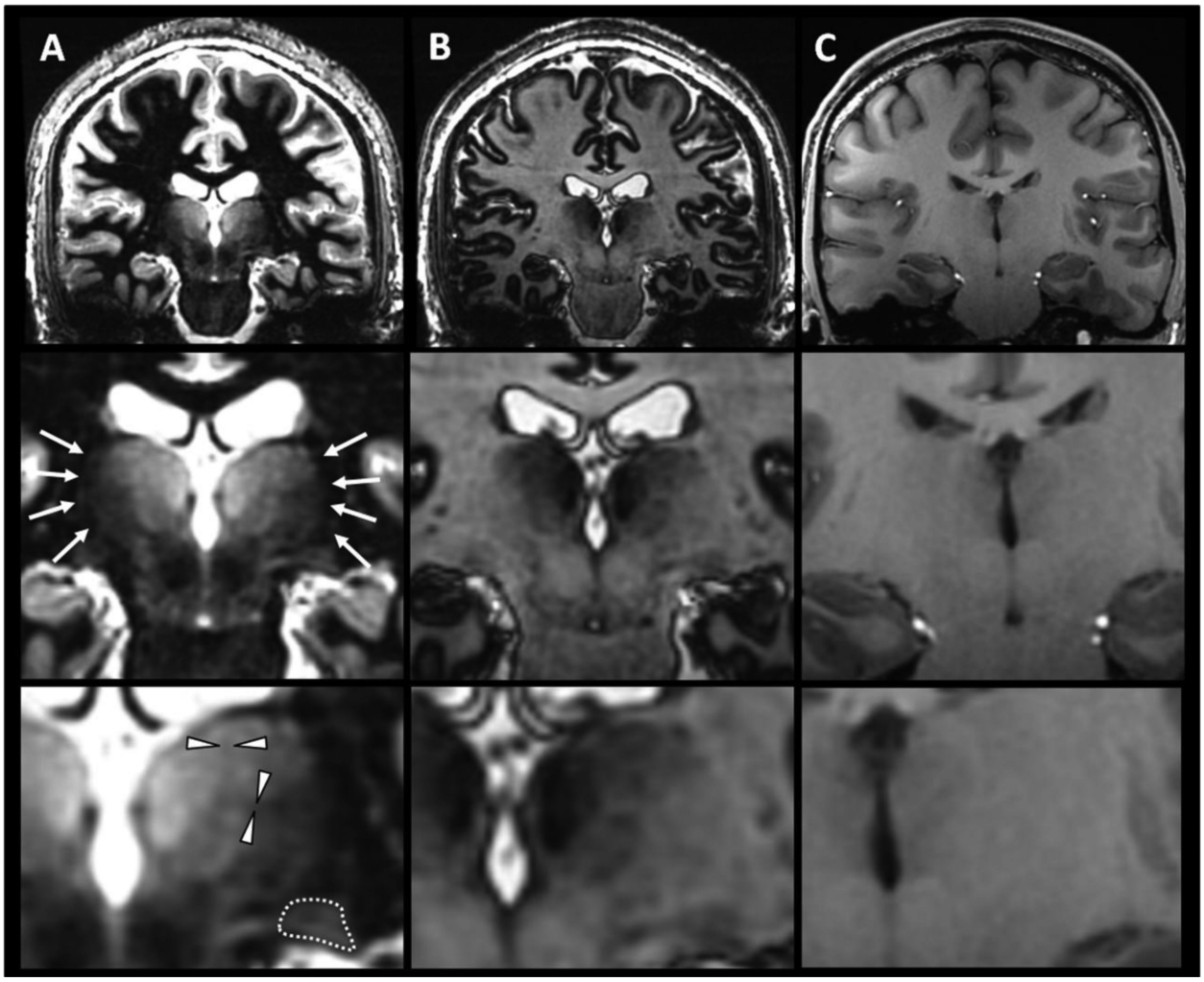


**Figure 3. Global regime of contrast – In vivo data**

Representative images at the WM null regime **(A)**, GM null regime **(B)** and with a standard MPRAGE protocol close to the CSF null regime **(C)**. The acquisition parameters for **(A)** and **(B)** were TS=5000ms, TI=730ms and 1080ms respectively, N=200, BW=25KHz, TR=9.8ms, TE=4ms, $\alpha$ =4°, resolution=1mm$^3$, ARC acceleration factor=2.5, NEX=1, scan time=6.8min. The standard MPRAGE protocol **(C)** recommended for morphometric analysis (Jack et al., 2008) was acquired with TS=3700ms, TI=1200ms, N=220, BW=15KHZ, TR=5.4ms, TE=2.4ms, $\alpha$ =10°, resolution 1mm$^3$, ARC acceleration factor=2.5, scan time=5 min.

In line with simulations, the higher signal and the better delineation of the external boundaries of the thalamus (arrows in **(A)** and dotted line at higher magnification delineating the lateral geniculate nucleus from the surrounding WM) were striking at the WM null regime compared to the GM null regime. Some thin hypointense boundaries believed to be attenuated WM lamellae separating adjacent nuclei, were only visible in the WM null regime (arrowheads at higher magnification). For comparison, the standard MPRAGE contrast provided a classical T1 weighted image but with still lower thalamic contrast **(C)**.

The WM null regime was preferred for the next steps of the optimization for thalamus segmentation.

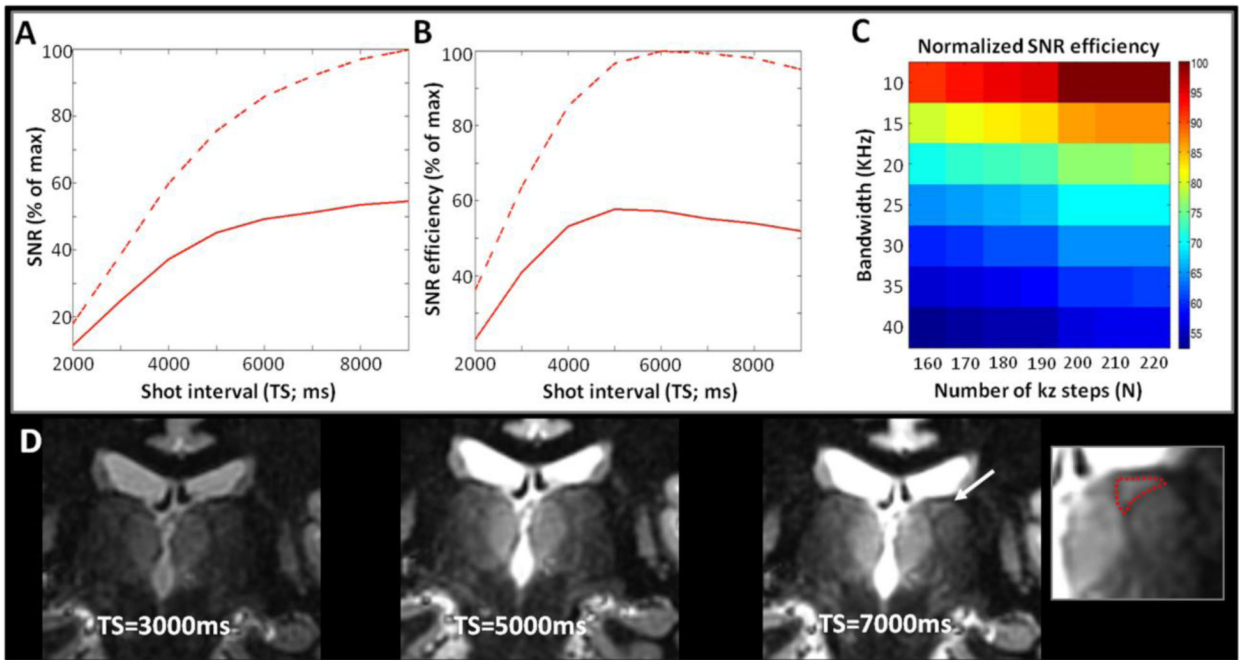


**Figure 4. Optimization of TS - N and BW - Signal**

The SNR **(A)** and SNR efficiency **(B)** were simulated as a function of TS effected by changing TD at the WM null regime with the MR parameters as described for **(D)** and with the higher range of intra-thalamic T1 (dashed) and the lower range of intra-thalamic T1 (solid), similar to **Figure 2** and as measured in **Figure 1**. The signal and signal efficiency were normalized to the maximum values. From the simulations, the signal is expected to increase along TS and the signal efficiency is expected to reach a plateau around TS=6000ms.

At the optimal TS of 6000ms, the map of SNR efficiency as a function of N and bandwidth **(C)** predicted higher SNR efficiency for higher N and lower bandwidth.

**(D):** Representative images acquired at three TS=3000ms, 5000ms and 7000ms, with TI computed to stay at the WM null regime in each case. Other parameters fixed at N=200, BW=20KHz, TR=9.8ms, TE=4ms, $\alpha$ =4°, resolution=1mm$^3$, ARC acceleration factor=2.5, NEX=1. Scan time=4.1min, 6.8min, and 9.6min respectively. The images are displayed at the same window and level. The experiments confirmed the gain in signal and contrast with TS. Structures such as the triangle of the lateral dorsal nucleus (LD; arrow and enlarged view at TS=7000ms) only became clearly visible at longer TS.

The WM null regime at TS=6000ms, N=200 and BW=20KHz was preferred for the next steps of the optimization for thalamus segmentation.

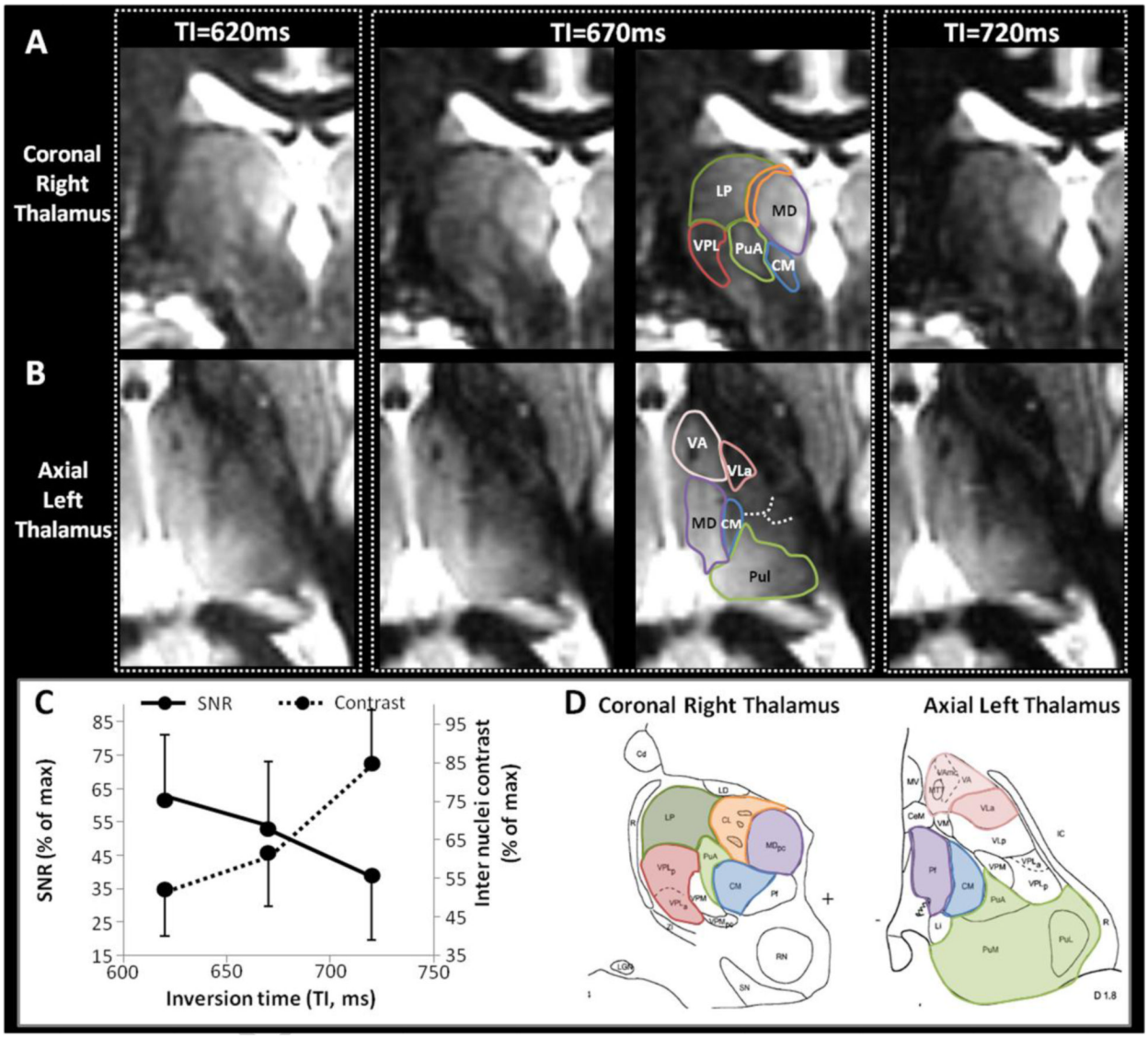


**Figure 5. Fine optimization of TI**

Different TI were tested around the WM nulling point for TS=6000ms. Representative coronal images of the right thalamus **(A)** and axial images of the left thalamus **(B)** at three different TIs close to the WM nulling point, as noted. Other parameters fixed at TS=6000ms, N=200, BW=15KHz, TR=10.2ms, TE=4.4ms, $\alpha$ =4°, resolution=1mm$^3$, ARC acceleration factor=2.5, NEX=1, scan time=8.2min. TI=670ms is shown without and with annotations. The average SNR and the average contrast between multiple pairs of adjacent nuclei were measured for each condition and plotted in **(C)**. The corresponding histological plates from the Morel atlas (Morel et al., 1997) are shown for anatomic correspondence in **(D)**.

From the simulations (see **Figure 2A and 2B**), the thalamic signal was expected to decrease with longer TI around the WM null regime, but the intra-thalamic contrast (relative difference between the signal curves for nuclei with low and higher T1 values) was expected to increase for longer TI around the WM null regime. Experimentally, the trade-off between thalamic signal and contrast along TI was confirmed **(C)**. Several nuclei were better delineated at TI 670ms. For example, on the coronal view **(A and D)** the hyperintensity of LP (green) and MD (purple) was distinct from the more hypointense VPL (red), CM (blue)

and CL (orange). Also, a thin hypointense border allowed a clear delineation of the PuA (green) that was not possible at TI=620ms due to insufficient contrast, nor at TI=720ms, due to insufficient signal. Similarly, on axial views **(B and D)**, the thin hypointense border delineating VA (pink) was better seen at TI=670ms. Same observation for the hypointense triangle corresponding to VLa (dark pink) seen at TI=670ms (and to a lesser extent at TI=620ms) but not individualized at TI=720ms due to the loss of signal from the adjacent posterior nuclei. Some subtle boundaries were also made out (dashed lines) and will be better emphasized by scanning without parallel imaging.

The WM null regime at TS=6000ms and TI=670ms was preferred for the next steps of the optimization for thalamus segmentation.

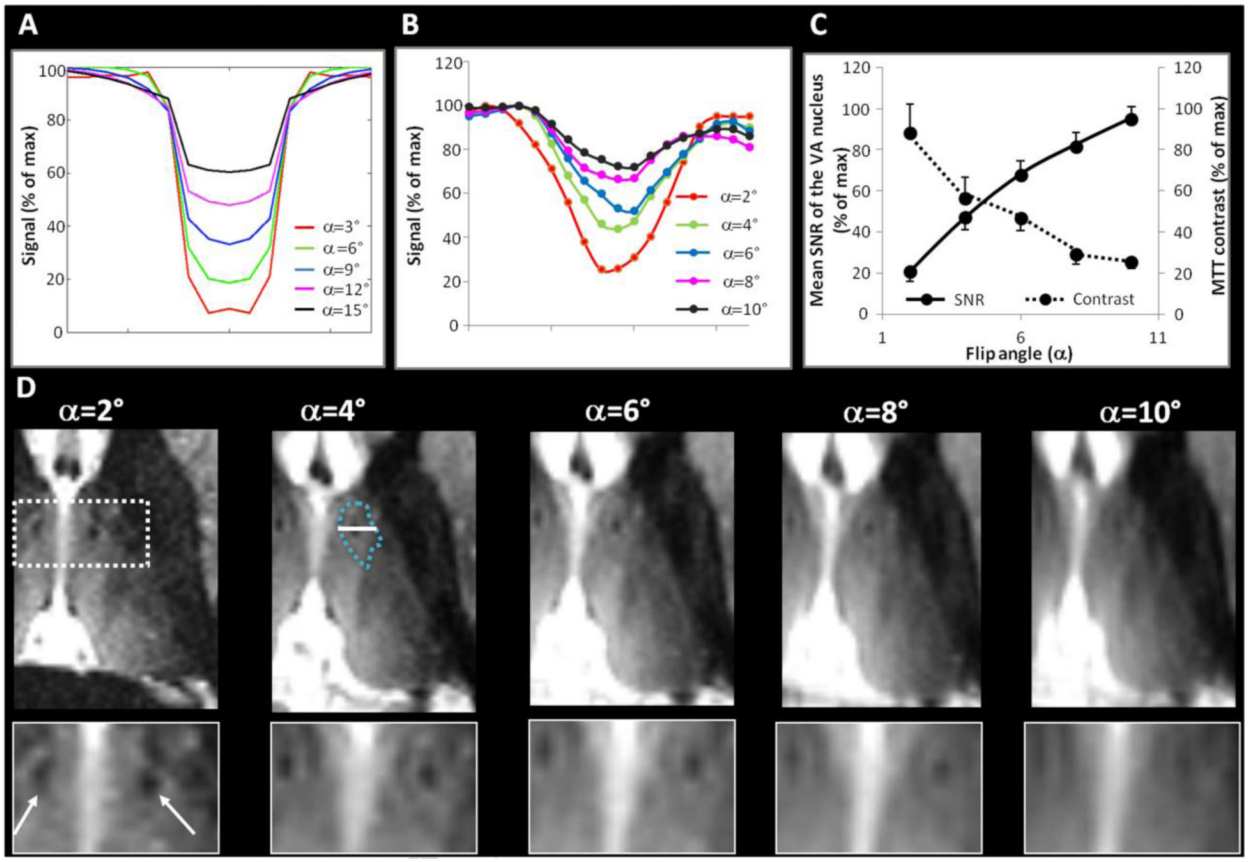


**Figure 6. Optimization of the flip angle (α)**

Simulated signal at the WM null regime of a structural 1D phantom consisting of few pixels of WM between larger regions of thalamic-like tissue **(A)**, with the MR parameters as described for **(D)**. Signal intensity profile measured along a line crossing the mammillothalamic tract (MTT, **B**) as illustrated on the α =4° image in **(D)**. In **(A)** and **(B)** the signal was normalized to the maximum value for each α. The SNR and the contrast of the MTT, a surrogate for image blur (see Methods), were also measured for each condition and plotted in **(C)**.

Representative images acquired at five different α **(D)**, with the other parameters fixed at TS=6000ms, TI=670ms, N=200, BW=20KHz, TR=6.9ms, TE=3.0ms, resolution=1mm$^3$, ARC acceleration factor=2.5, NEX=1, scan time=8.2min. The images are axial reconstructions from a coronal acquisition and are displayed at the same window and level. Enlarged views of the mammillothalamic tract (MTT, arrows) are shown for each α.

From the simulations **(A)**, the signal of a small structure embedded in another tissue is expected to progressively fade at higher α (shallower profile and gentler slope). This effect was particularly relevant experimentally with increased blur along the slice direction (antero-posterior) that obscured small structures embedded in a larger region, such as the MTT or the small hypointense borders delineating adjacent nuclei (the hypointense border of the ventral anterior nucleus was delineated in cyan at α =4° for illustration). The signal profile of the MTT measured experimentally matched the simulations **(B)** and the trade-off between thalamic signal and blur along α was confirmed **(C)**. α =4° represented the best trade-off to keep these thin structures visible with sufficient signal.

The WM null regime at TS=6000ms, TI=670ms, and α =4° was preferred for the optimization for thalamus segmentation.

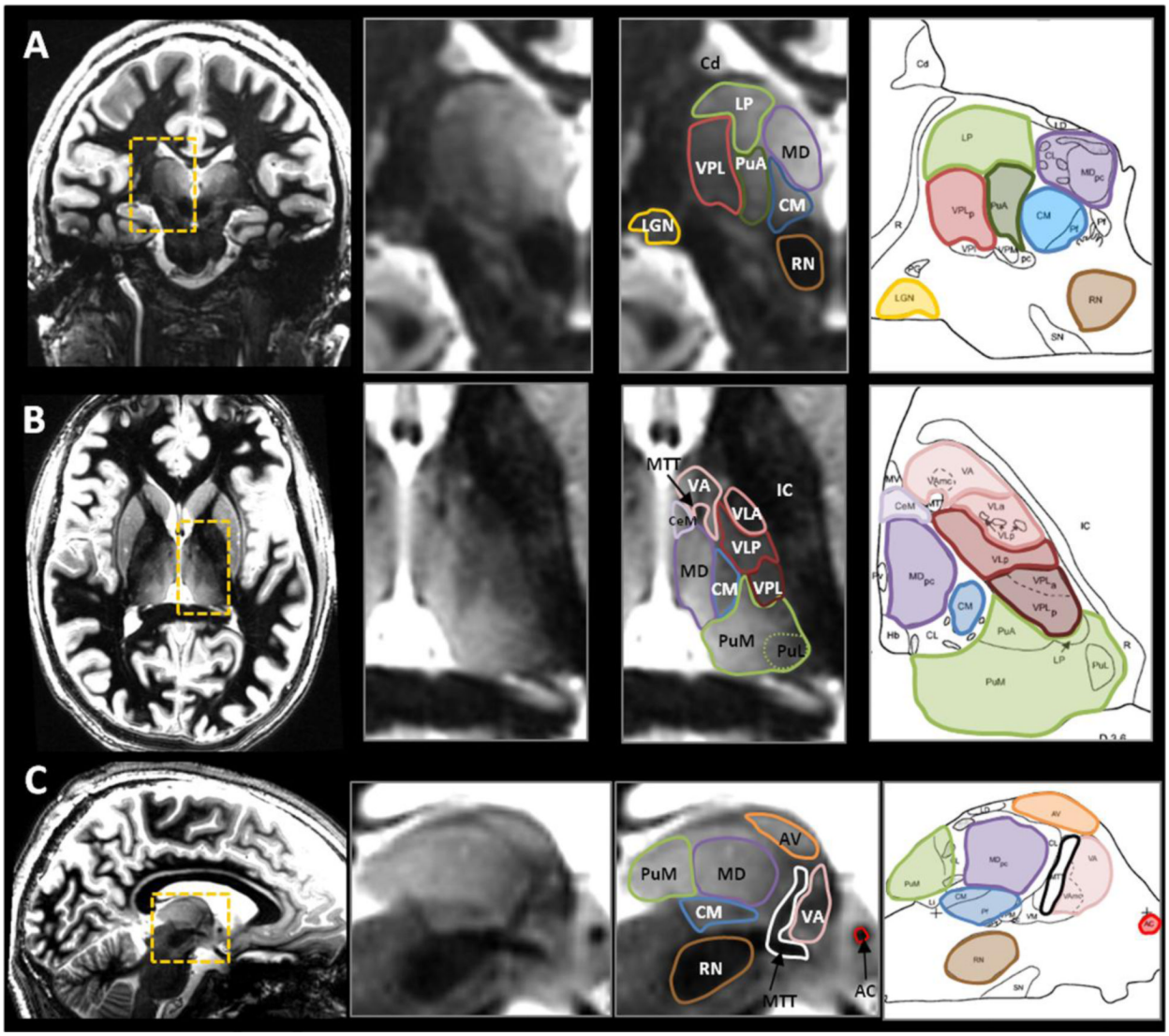


**Figure 7. Visualization of thalamic nuclei compared with histological plates**

Representative examples of MR scans in the 3 orthogonal orientations (each orientation shown in a different volunteer) and presented with the corresponding histological plates (Morel et al., 1997). Several nuclei can be identified thanks to enhanced intrinsic contrast between adjacent structures. Also, thin hypointense bands helped to isolate structures with otherwise close signal. For example, see the thin boundaries around the pulvinar anterior (PuA, green) in coronal **(A)**, around the ventral anterior nucleus (VA, pink) in axial **(B)**, and around the anterior ventral nucleus (AV, orange) in sagittal **(C)**. Good correspondence between MR boundaries and the atlas can be observed.

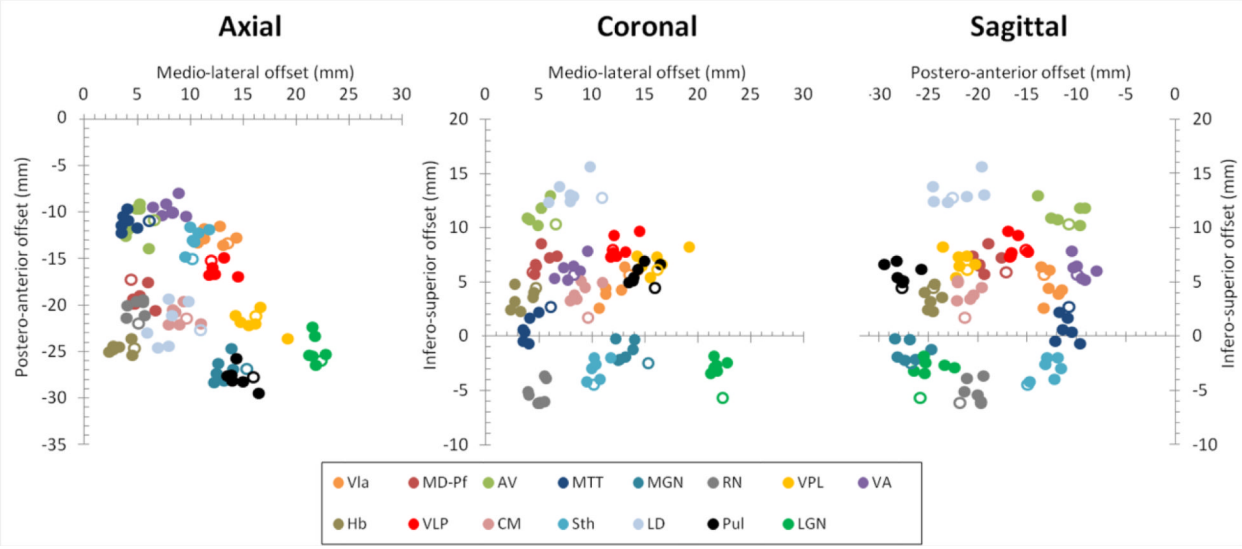


**Figure 8. Scatter plots of MR-based and atlas-based center of mass of thalamic nuclei**

The Talairach center of mass (COM) coordinates of 15 structures (abbreviations as described in the Methods) in 6 volunteers are plotted in axial, coronal and sagittal projections. The atlas-based Talairach COM coordinates are shown with open icons. The middle of the anterior commissure is at the origin (0,0,0). Good agreement was observed between the individuals and with the atlas.

## Table 1

Tissue parameters used for simulations

| Tissue parameters | T1 [a] | PD | T2* [d] |
|---|---|---|---|
| WM | 1201 ms | 0.71 [b] | 28.7 ms |
| Cortical GM | 1962 ms | 0.81 [b] | 31.4 ms |
| Pulvinar - Mediodorsal nuclei | 1800 ms | 0.79 [c] | 24.2 ms |
| Center median - Ventral posterior lateral | 1400 ms | 0.74 [c] | |

[a] The T1 were from our measurements (see section 3.1 and Figure 1)

[b] The proton density (PD) for WM and GM were taken from the literature (Neeb et al., 2006)

[c] The PD for the thalamic nuclei were estimated based on the relationship between T1 and PD: 1/PD = A+B/T1 (Volz et al., 2012).

[d] The T2* values were derived from the literature (Deistung et al., 2013) and used to model the variable signal decay induced by variation of TE that comes with changing BW.